


Cite this: *RSC Adv.*, 2020, 10, 3554

# Chemoselective reduction of nitro and nitrile compounds using an Fe<sub>3</sub>O<sub>4</sub>-MWCNTs@PEI-Ag nanocomposite as a reusable catalyst

Sara Ansari,<sup>a</sup> Alireza Khorshidi <sup>\*a</sup> and Shahab Shariati<sup>b</sup>

Multi-walled carbon nanotubes (MWCNTs) were modified with carboxylic acid functional groups (MWCNTs-(COOH)<sub>n</sub>) prior to decoration with Fe<sub>3</sub>O<sub>4</sub> nanoparticles. A further modification step by polyethyleneimine (PEI) resulted in Fe<sub>3</sub>O<sub>4</sub>-MWCNTs@PEI which provided a suitable platform for coordination and *in situ* reduction of silver ions to obtain an Fe<sub>3</sub>O<sub>4</sub>-MWCNTs@PEI-Ag nanocomposite with highly dispersed Ag nanoparticles. The Fe<sub>3</sub>O<sub>4</sub>-MWCNTs@PEI-Ag hybrid material was characterized by various techniques such as Fourier transform infrared spectroscopy (FT-IR), X-ray diffraction (XRD), transmission electron microscopy (TEM), vibrating sample magnetometry (VSM), X-ray photoelectron spectroscopy (XPS) and thermogravimetric analysis (TGA), and was used as an efficient catalyst for chemoselective reduction of nitroaromatic and nitrile compounds to their corresponding amines in aqueous solution at ambient temperature. Nitrofurazone, a cytotoxic antibiotic, as a non-aromatic example was also reduced selectively at the nitro group without reduction of the other functionalities in the presence of Fe<sub>3</sub>O<sub>4</sub>-MWCNTs@PEI-Ag. The catalyst was magnetically recoverable and maintained its activity for at least six cycles without considerable loss of efficiency.

Received 16th November 2019

Accepted 16th January 2020

DOI: 10.1039/c9ra09561f

rsc.li/rsc-advances

## Introduction

Silver nanoparticles (Ag NPs) have been of special interest for many decades due to their diverse applications in a variety of fields such as biology,<sup>1,2</sup> electronics<sup>3,4</sup> and catalysis.<sup>5,6</sup> Among the noble metal nanoparticles, silver nanoparticles have attracted specific attention due to their potential as catalysts in various transformations.<sup>7,8</sup> As catalysts, the performance of Ag NPs is associated with some limitations. These include, but are not limited to, problematic separation of the catalyst from products by traditional methods, aggregation of nanoparticles and stability issues.<sup>9</sup> In order to overcome these limitations, various supports have been devised to immobilize Ag NPs. A few examples include carbon materials,<sup>10,11</sup> silica,<sup>12</sup> alumina,<sup>13</sup> silica nanotubes, carbon nanofibers, polymers and metal oxides.<sup>14,15</sup> Immobilization of Ag NPs on the surface of such supports plays an important role in higher stability and catalytic activity and paves the way for their easy separation from different reaction media.<sup>16</sup> Nitroaromatic compounds, on the other hand, are widely used in various industries such as plastics, dyeing, agriculture, *etc.*<sup>17</sup> It has been proved that even trace amounts of these compounds can pose an adverse effect on the environment and human health. Hence, several investigations have been carried out to eliminate or convert

nitroaromatic compounds to less harmful products.<sup>18,19</sup> Aromatic and aliphatic amines are among the most important intermediates in the synthesis of pharmaceuticals, dyes, surfactants, anti-foam agents, corrosion inhibitors, and polymers,<sup>20–23</sup> and can be obtained from direct reduction of nitro compounds. Also, many important compounds such as amides, imines, azo compounds, isocyanates and diazonium salts can be prepared from amines.<sup>24,25</sup> Although, various methods have been designed for the synthesis of aromatic and aliphatic amines from nitro precursors, most of them have serious drawbacks such as production of large quantities of waste, which in turn can lead to very serious environmental and health hazards.<sup>26</sup> Metal complexes have been used as catalyst for reduction of nitroaromatic compounds to aromatic amines.<sup>27,28</sup> However, they have their own disadvantages such as production of noxious waste and recyclability issues. On the other hand, reduction of nitrile compounds by NaBH<sub>4</sub> or LiAlH<sub>4</sub> usually leads to the production of amides instead of amines and therefore they cannot provide chemoselectivity.<sup>29</sup> Hence, study on effective and green methodologies for chemoselective transformation of nitrile and nitro compounds to amines is still of a great interest. In recent years, the abundance of published reports on the application of multi-walled carbon nanotubes (MWCNTs) is testimony to the considerable attention to functionalization of these carbon scaffolds for various applications such as oxidative dehydrogenation,<sup>30–32</sup> sensors for determination of DNA,<sup>33</sup> and MRI contrast agents.<sup>34</sup> Due to high surface area, unique chemical and

<sup>a</sup>Department of Chemistry, Faculty of Sciences, University of Guilan, P. O. Box: 41335-1914, Iran. E-mail: Khorshidi@guilan.ac.ir; Tel: +989113397159

<sup>b</sup>Department of Chemistry, Rasht Branch, Islamic Azad University, Rasht, Iran


physical properties, high resistance and accessibility, CNTs have been used as outstanding supports for deposition of nanoparticles or metal complexes, to prepare stable and recoverable heterogeneous catalysts for various reactions.<sup>35–37</sup> However, CNTs cannot be easily separated from the reaction mixture because they can stay suspended for a long time.<sup>38</sup> To overcome this problem, the researchers found that attachment of magnetic nanoparticles to them may prevent their dispersion in solution. These new magnetic hybrids have attracted considerable attention due to their recyclability from the solution by using an external magnet and purification of the target products by an easy workup.<sup>39,40</sup> In addition, while there are interesting achievements with noble metal functionalized magnetic carbon nano/microtubes, for example, in catalysis and sensors,<sup>41–43</sup> other low dimensional nanocarbon scaffolds are actively pursued by the researchers,<sup>44–50</sup> and are going to find application in energy materials.<sup>51–60</sup>

Herein, we introduce  $\text{Fe}_3\text{O}_4\text{-MWCNTs@PEI}$  as a novel support for uniform dispersion of Ag NPs over its surface, and application of the  $\text{Fe}_3\text{O}_4\text{-MWCNTs@PEI-Ag}$  hybrid material as an efficient catalyst for chemoselective reduction of nitro and nitrile compounds to amines in aqueous solution under very mild and green conditions.

## Experimental

### Materials and methods

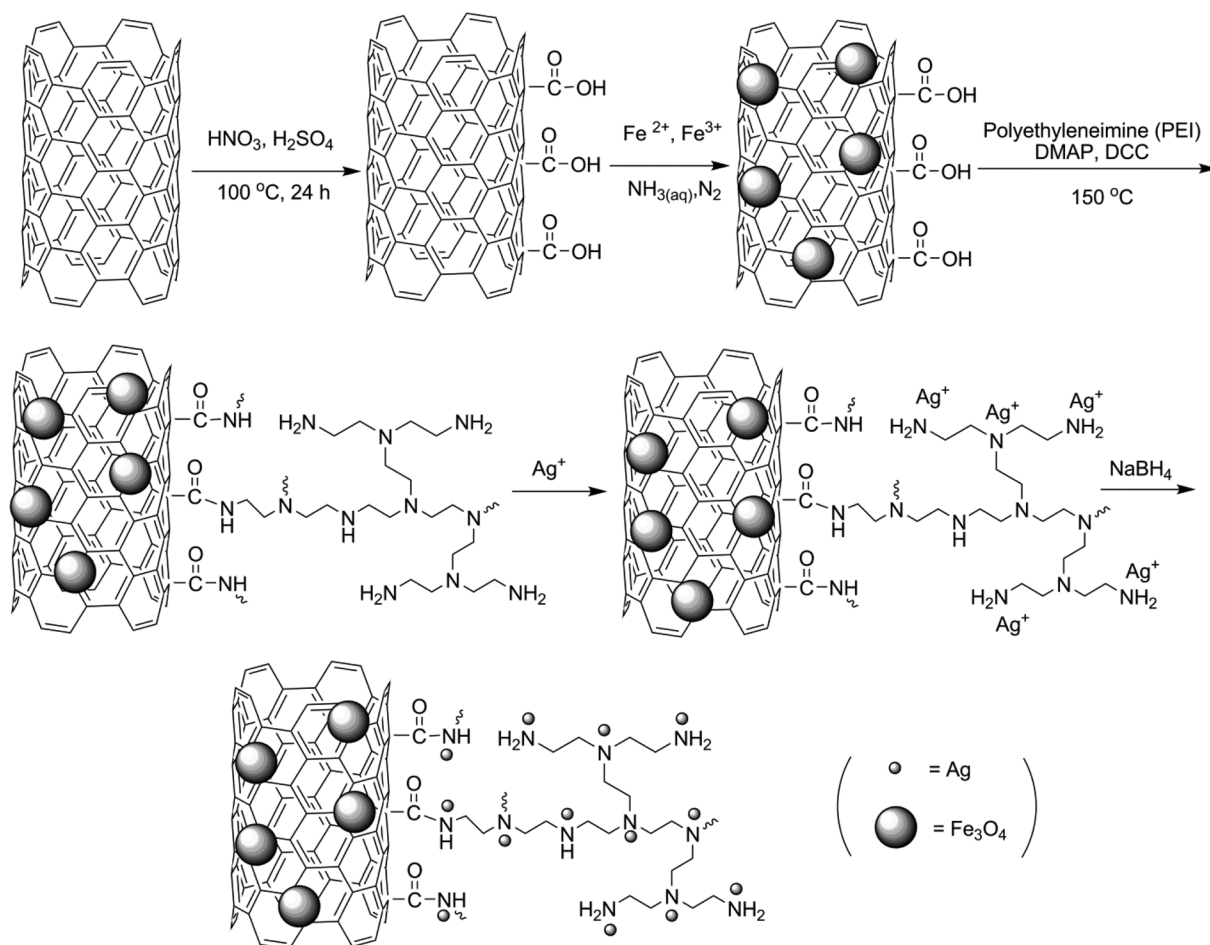
MWCNTs were purchased from Cheap-Tube Inc., USA. Ferric chloride hexahydrate ( $\text{FeCl}_3 \cdot 6\text{H}_2\text{O}$ ) and ferrous sulfate heptahydrate ( $\text{FeSO}_4 \cdot 7\text{H}_2\text{O}$ ) were purchased from Fluka. All of the other chemicals were purchased from Sigma-Aldrich and were used as received.

### Synthesis of acid functionalized multi-walled carbon nanotubes, $\text{MWCNTs}(\text{COOH})_n$

$\text{MWCNTs}(\text{COOH})_n$  was synthesized as follows: 1.0 g of the MWCNTs was added to 20 mL of a mixture of  $\text{HNO}_3$  and  $\text{H}_2\text{SO}_4$  (v/v 1 : 3). The mixture was then refluxed under stirring at 100 °C for 24 h and after cooling down to room temperature, it was diluted with distilled water in an ice bath. Successive rinsing with distilled water by means of a centrifuge until neutral pH resulted in a black precipitate which was dried at 85 °C for 24 h under vacuum.

### Synthesis of $\text{Fe}_3\text{O}_4\text{-MWCNTs}(\text{COOH})_n$

First, a dispersion of the  $\text{MWCNTs}(\text{COOH})_n$  in distilled water (0.125 g in 80 mL) was prepared. Then a solution of  $\text{FeSO}_4 \cdot 7\text{H}_2\text{O}$



Scheme 1 Stepwise synthesis of  $\text{Fe}_3\text{O}_4\text{-MWCNTs@PEI-Ag}$ .

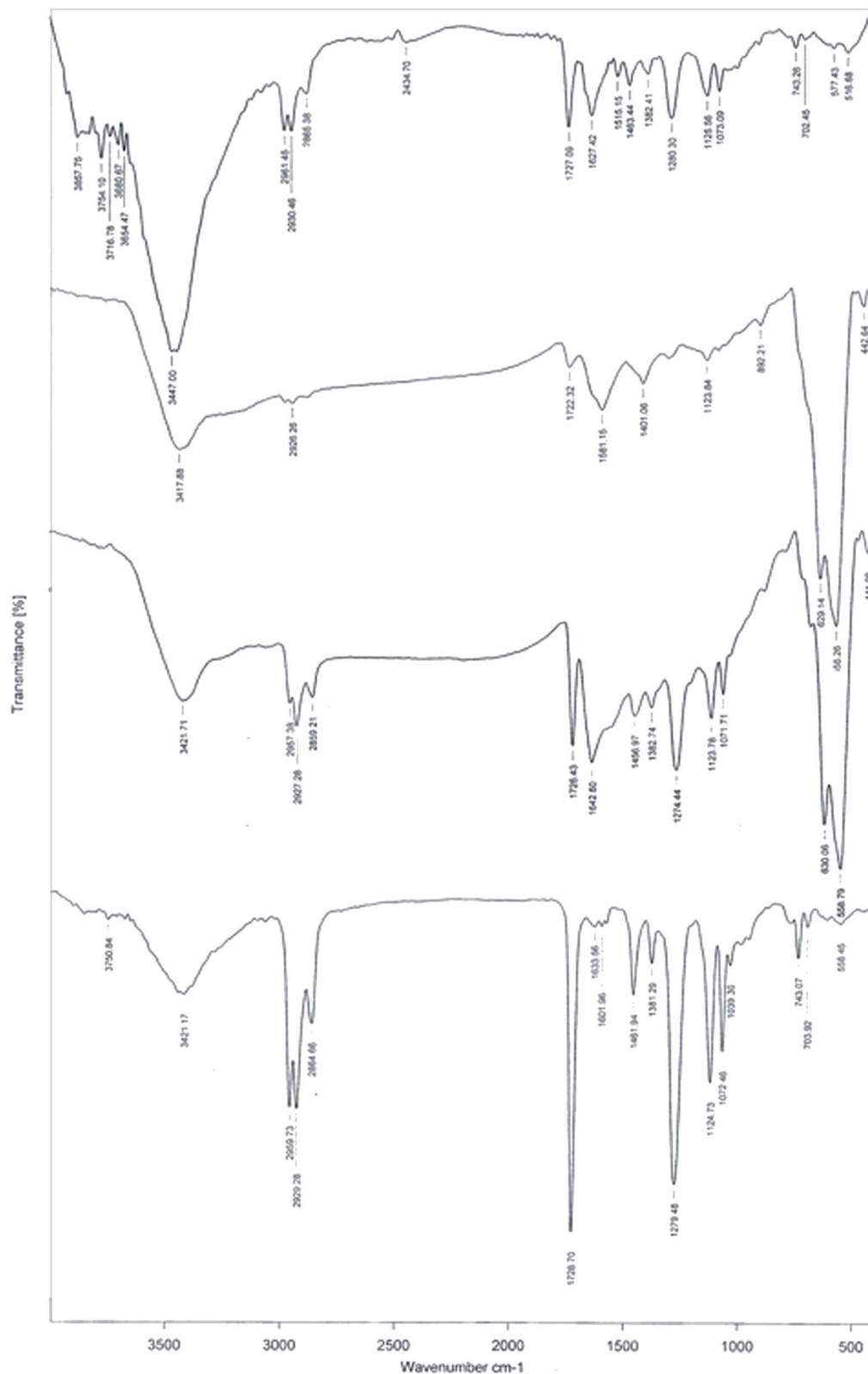


Fig. 1 From top to bottom: FTIR spectra of MWCNTs-(COOH)<sub>n</sub>, Fe<sub>3</sub>O<sub>4</sub>-MWCNTs-(COOH)<sub>n</sub>, Fe<sub>3</sub>O<sub>4</sub>-MWCNTs@PEI, and Fe<sub>3</sub>O<sub>4</sub>-MWCNTs@PEI-Ag.

and FeCl<sub>3</sub>·6H<sub>2</sub>O in water (2.11 mmol, 4.47 mmol, 150 mL) was prepared and added to the above dispersion. The mixture was then placed in an ultrasonic bath for 15 min in order to achieve

a uniform distribution of metal ions over the surface of MWCNTs-(COOH)<sub>n</sub>. The resulting mixture was then stirred under N<sub>2</sub> atmosphere at 90 °C for 40 min. In the next step,



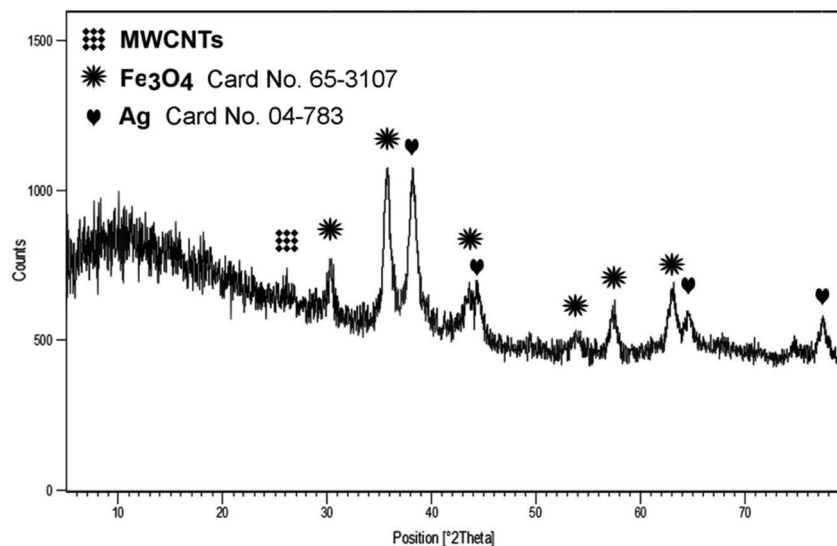


Fig. 2 XRD pattern of the  $\text{Fe}_3\text{O}_4$ -MWCNTs@PEI-Ag nanocomposite.

15 mL of a 1.5 M ammonia solution was added dropwise. Stirring was continued for 3 h at 90 °C under  $\text{N}_2$  atmosphere. Finally, the product was separated by an external magnet and washed with water until neutral pH was achieved. The product was dried in an oven at 80 °C overnight.

#### Synthesis of $\text{Fe}_3\text{O}_4$ -MWCNTs@PEI

0.15 g of  $\text{Fe}_3\text{O}_4$ -MWCNTs- $(\text{COOH})_n$  was dispersed in 10 mL of DMF by sonication in an ultrasonic bath for 15 min. Then, a solution of PEI (0.1 g in 5 mL of DMF) was prepared by sonication for 15 min and added at once to the above mentioned suspension. Afterward, 0.2 g of 4-(dimethylamino) pyridine (DMAP) and 0.25 g of *N,N*-dicyclohexylcarbodiimide (DCC) were added to the above mixture. The mixture was then refluxed for 60 h at 150 °C. Finally, the  $\text{Fe}_3\text{O}_4$ -MWCNTs@PEI was separated by an external magnet and washed with DMF ( $2 \times 3$  mL), then dried in vacuum at 90 °C.

#### Synthesis of $\text{Fe}_3\text{O}_4$ -MWCNTs@PEI-Ag

Deposition of silver nanoparticles over the surface of  $\text{Fe}_3\text{O}_4$ -MWCNTs@PEI was achieved by coordination of  $\text{Ag}^+$  ions by  $-\text{NH}_2$  functional groups of PEI and reduction with  $\text{NaBH}_4$ .

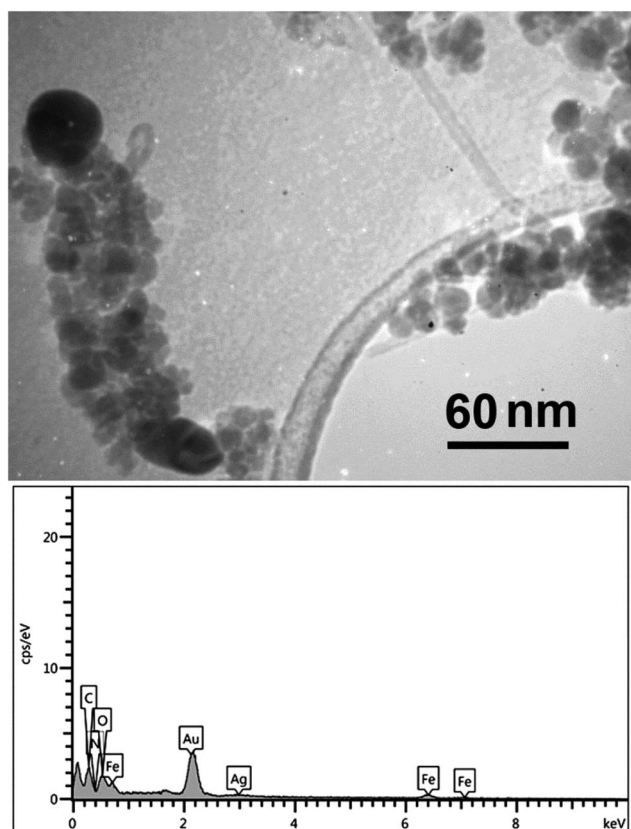


Fig. 3 TEM image of the  $\text{Fe}_3\text{O}_4$ -MWCNTs@PEI-Ag nanocomposite (top), and the corresponding EDX analysis (bottom).

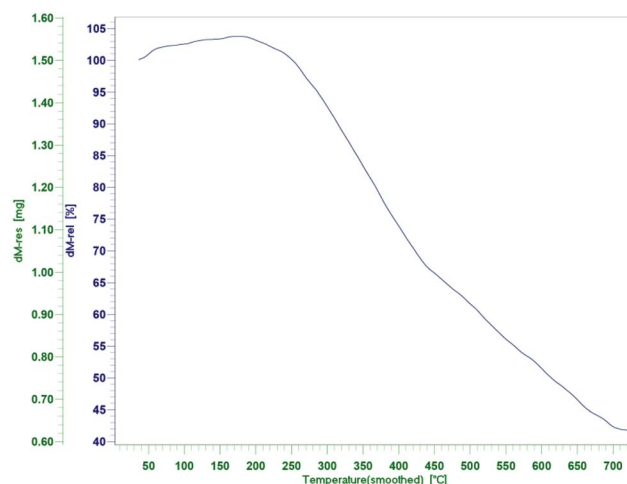


Fig. 4 TGA curve for the  $\text{Fe}_3\text{O}_4$ -MWCNTs@PEI-Ag composite.





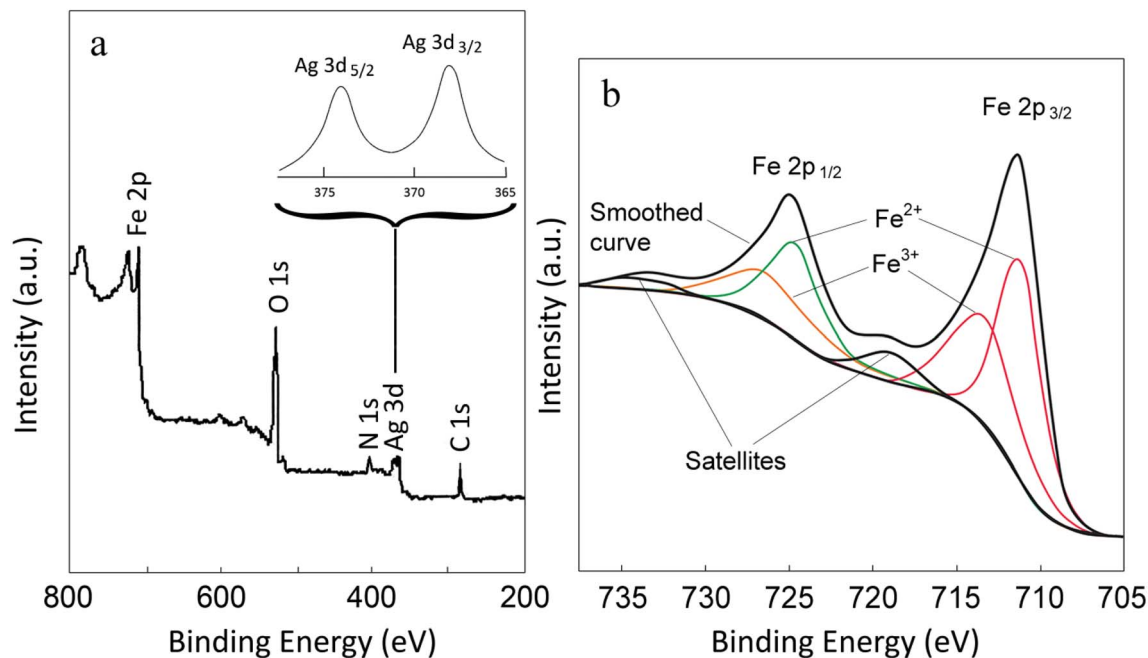


Fig. 5 XPS survey scan for the  $\text{Fe}_3\text{O}_4\text{-MWCNTs@PEI-Ag}$  composite (a), and high-resolution Ag 3d (inset) and Fe 2p (b) signals.

Briefly, 50 mg of  $\text{Fe}_3\text{O}_4\text{-MWCNTs@PEI}$  was dispersed in 200 mL of deionized water by ultrasound irradiation for 4 min. Then, 8.0 mg of  $\text{AgNO}_3$  was added to the mixture under vigorous

stirring by a mechanical stirrer at 1800 rpm. Afterward, 3 mL of 100 mM  $\text{NaBH}_4$  solution was injected at once to the mixture and the reaction continued for 3 h at room temperature. The resulted product was separated and washed with deionized water and acetone and dried in vacuum at 60 °C.

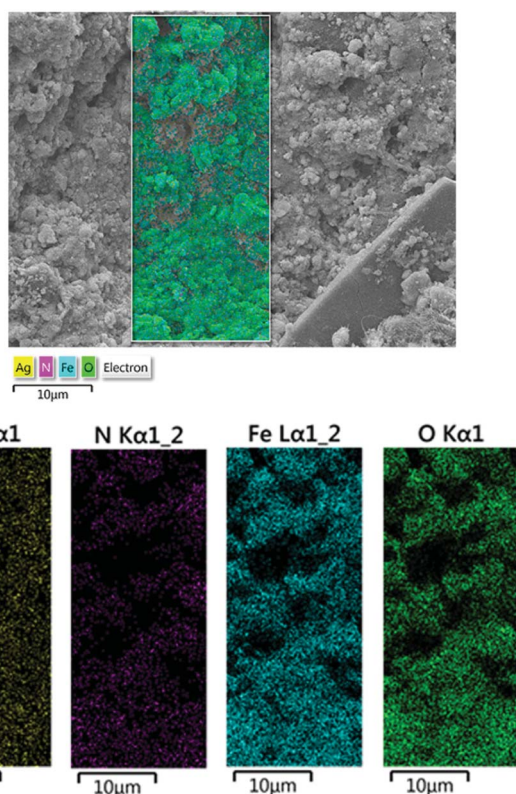


Fig. 6 Mapping analysis of the  $\text{Fe}_3\text{O}_4\text{-MWCNTs@PEI-Ag}$  composite.

#### General procedure for reduction of aromatic nitro and nitrile compounds by $\text{Fe}_3\text{O}_4\text{-MWCNTs@PEI-Ag}$ as catalyst

To 100 mL of a 1.0 mM aqueous solution of the corresponding nitroaromatic compound, 3 mL of freshly prepared  $\text{NaBH}_4$  solution (0.1 M) and 1.0 mg of  $\text{Fe}_3\text{O}_4\text{-MWCNTs@PEI-Ag}$  were added and the mixture was stirred by means of a mechanical stirrer at room temperature. Trend of reduction of nitro groups was monitored by using a UV-Vis spectrophotometer according

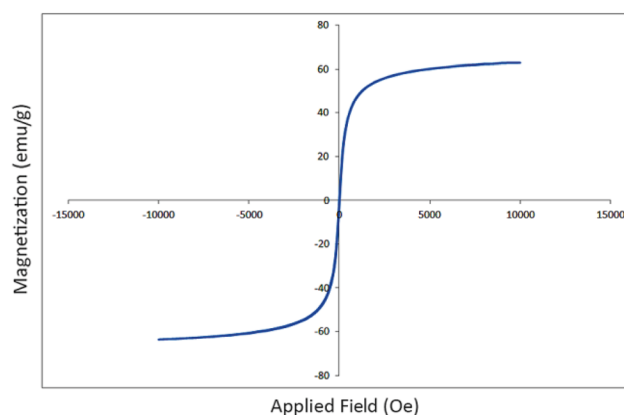


Fig. 7 Hysteresis curve for  $\text{Fe}_3\text{O}_4\text{-MWCNTs@PEI-Ag}$  composite measured at 300 K.



**Table 1** Effect of the catalyst amount on the reduction efficiency for 4-nitroaniline

Entry <sup>a</sup>	Catalyst amount (mg)	Yield of benzene-1,4-diamine (%)	Apparent rate constant, $k$ (min <sup>-1</sup> )
1	0 mg	Negligible	—
2	1.3 mg	94.43%	0.188 min <sup>-1</sup>
3	1.0 mg	90.72%	0.152 min <sup>-1</sup>
4	0.7 mg	69.17%	0.073 min <sup>-1</sup>

<sup>a</sup> All of the reactions were carried out according to the general experimental procedure at room temperature.

**Table 2** Effect of pH on the reduction of 4-nitroaniline

Entry <sup>a</sup>	pH	Reduction efficiency (%)	Apparent rate constant, $k$ (min <sup>-1</sup> )
1	5.0	31.0%	0.031 min <sup>-1</sup>
2	7.0	90.7%	0.152 min <sup>-1</sup>
3	10.0	67.9%	0.077 min <sup>-1</sup>

<sup>a</sup> All of the reactions were carried out according to the general experimental procedure at room temperature.

to the following procedure. After removal of the catalyst by an external magnet, a small portion of the solution was sampled in a quartz cuvette and the absorption of the solution was measured at the appropriate  $\lambda_{\text{max}}$ . In the case of aromatic nitriles, 0.1 mmol of the corresponding aromatic nitrile compound was added to 10 mL of distilled water. Then, 1 mg of Fe<sub>3</sub>O<sub>4</sub>-MWCNTs@PEI-Ag was added and the mixture was sonicated for 5 min. Then, 3 mL of freshly prepared NaBH<sub>4</sub> solution (0.2 M) was added and the mixture was refluxed at 110 °C in an oil bath. The progress of the reaction was monitored by gas chromatography.

### Characterization techniques

FT-IR spectra were recorded on a Bruker ALPHA spectrometer from 500 to 4000 cm<sup>-1</sup> using KBr pellets. UV-Vis spectra were recorded on a PerkinElmer LAMBDA 25 spectrophotometer. XRD patterns were recorded on a Philips X'pert diffractometer with mono chromatized Cu K $\alpha$  radiation at 40 kV and 20 mA (Ni filter,  $2\theta$  10 to 70° with a step size of 0.05° and a count time of 1 s). TEM images were obtained on a transmission electron microscope (TEM, Philips MC 10) with an acceleration voltage of 80 kV. Thermogravimetric analysis (TGA) was performed on a STA 1500 instrument at a heating rate of 10 °C min<sup>-1</sup> in air atmosphere. GC analyses were performed on a GC Chrom from Teif Gostar Faraz Co., Iran (split/splitless injector, capillary SAB-5 column, FID detector, N<sub>2</sub> as carrier gas with flow rate of 0.8 mL min<sup>-1</sup>, column temp: 260 °C).

## Results and discussion

### Characterization of the nanocatalyst

Stepwise modification of MWCNTs with (i) -COOH functional groups, (ii) Fe<sub>3</sub>O<sub>4</sub> nanoparticles, (iii) covalent bonding of PEI, and (iv) decoration with Ag nanoparticles is illustrated in Scheme 1.

MWCNTs were functionalized with -COOH groups prior to the synthesis of Fe<sub>3</sub>O<sub>4</sub>, because magnetite nanoparticles cannot tolerate the strong acidic conditions required for acid modification. In the next step, covalent grafting of PEI was performed to prepare an appropriate medium for coordination of Ag<sup>+</sup> ions before they were reduced with NaBH<sub>4</sub>. This strategy resulted in a more uniform dispersion of Ag nanoparticles over the surface of the catalyst. Fig. 1 compares FTIR spectra of Fe<sub>3</sub>O<sub>4</sub>-MWCNTs@PEI-Ag with its individual components. The absorption band at 558 cm<sup>-1</sup> is attributed to the Fe-O

**Table 3** Effect of NaBH<sub>4</sub> concentration on the reduction of 4-nitroaniline

Entry <sup>a</sup>	NaBH <sub>4</sub> concentration (M)	Reduction efficiency%
1	0.3 M	93.11%
2	0.2 M	90.72%
3	0.1 M	72.88%

<sup>a</sup> All of the reactions were carried out according to the general experimental procedure at room temperature.

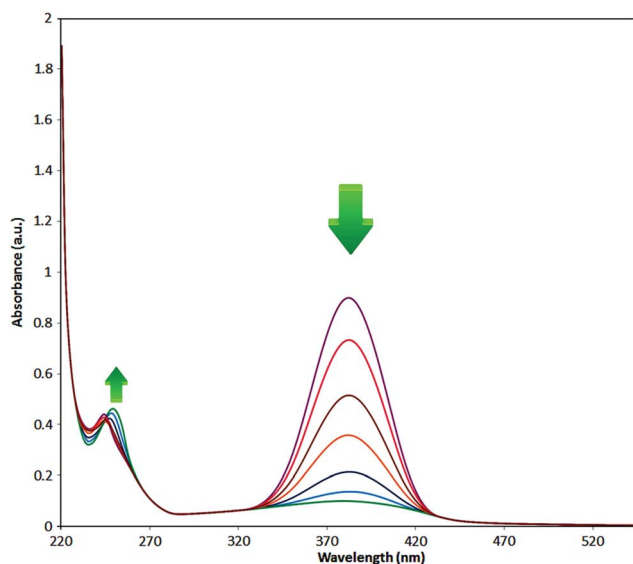
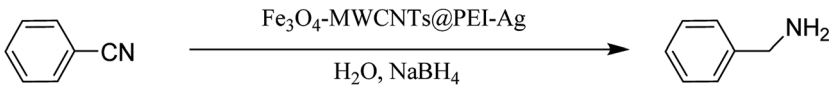
**Fig. 8** Trend of reduction for 4-nitroaniline at pH 7.0.

Table 4 Variety of nitroaromatic compounds reduced by Fe<sub>3</sub>O<sub>4</sub>-MWCNTs@PEI-Ag as the catalyst

Entry <sup>a</sup>	Nitroaromatic compound	Product	<i>k</i> <sub>app</sub> (min <sup>-1</sup> )	Time (min)
1			0.151	10
2			0.22	8
3			0.152	15
4			0.288	12
5			0.085	15
6			0.115	14
7			0.099	12
8			0.151	10
9			0.206	8
10			0.122	12

<sup>a</sup> All of the reactions were carried out according to the general experimental procedure.

**Table 5** Optimization of the reaction conditions for reduction of benzonitrile by Fe<sub>3</sub>O<sub>4</sub>-MWCNTs@PEI-Ag as catalyst in aqueous solution

				
Entry <sup>a</sup>	Catalyst amount (mg)	Time (min)	Temperature (°C)	Yield <sup>b c</sup> (%)
1	—	40	110	—
2	1.3	40	110	97%
3	1.0	40	110	95%
4	0.7	40	110	90%
5	1.0	30	110	87%
6	1.0	50	110	95%
7	1.0	40	90	83%
8	1.0	40	70	66%

<sup>a</sup> Reaction conditions: 0.1 mmol of benzonitrile and 0.6 mmol of NaBH<sub>4</sub>. <sup>b</sup> Isolated yield. <sup>c</sup> The product was characterized from its <sup>1</sup>HNMR spectroscopic data in comparison with authentic samples.

stretching vibrations in all of the Fe<sub>3</sub>O<sub>4</sub> containing intermediates and the final product.<sup>61</sup> Broad peaks at about 3400 cm<sup>-1</sup> may be attributed to either O–H stretching vibrations of –COOH in MWCNTs-(COOH)<sub>n</sub> and Fe<sub>3</sub>O<sub>4</sub>-MWCNTs-(COOH)<sub>n</sub>, or N–H stretching vibrations in Fe<sub>3</sub>O<sub>4</sub>-MWCNTs@PEI and Fe<sub>3</sub>O<sub>4</sub>-MWCNTs@PEI-Ag. A more convincing evidence on presence of –COOH, however, is the characteristic vibration of C=O at 1720 cm<sup>-1</sup>. In the case of Fe<sub>3</sub>O<sub>4</sub>-MWCNTs@PEI and Fe<sub>3</sub>O<sub>4</sub>-MWCNTs@PEI-Ag, on the other hand, characteristic vibrations that confirm covalent grafting of PEI are as follows: 1642 cm<sup>-1</sup> (amide carbonyl vibration), 1456 cm<sup>-1</sup> (N–H bending), 2959 cm<sup>-1</sup> and 2927 cm<sup>-1</sup> (aliphatic C–H stretching).<sup>62,63</sup>

Fig. 2 shows the XRD pattern of Fe<sub>3</sub>O<sub>4</sub>-MWCNTs@PEI-Ag. The low intensity reflection at 2θ 26.2 correspond to (002) plane of the multi-walled carbon nanotubes with graphite-like frame.<sup>64</sup> Six peaks at 2θ 30.2°, 35.7°, 43.7°, 53.87°, 57.5° and 62.9° correspond to (220), (311), (400), (422), (511) and (440) planes of crystalline Fe<sub>3</sub>O<sub>4</sub> magnetic nanoparticles, respectively (JCPDS file no. 65-3107).<sup>37</sup> Also, peaks at 2θ 38.3°, 44.3°, 64.8°, and 77.5° can be well attributed to (111), (311), (220) and (200) planes of face-centered-cubic (FCC) silver on the basis of standard values in the card (JCPDS file no. 04-783).

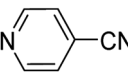
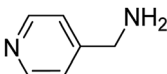
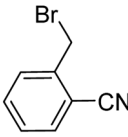
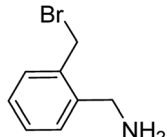
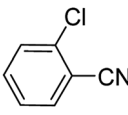
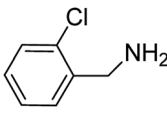
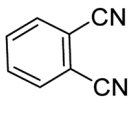
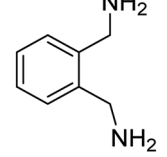
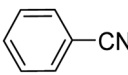
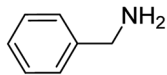
TEM imaging clearly revealed the presence of Fe<sub>3</sub>O<sub>4</sub> and Ag as nano-sized particles over the walls of nanotubes. In Fig. 3 (top), a fully decorated nanotube and a partially decorated one is captured. As it is shown, Fe<sub>3</sub>O<sub>4</sub> nanoparticles can be easily identified from their larger size (25–50 nm vs. 5–10 nm) and higher opacity in comparison with Ag nanoparticles. Due to the inherent limitations of co-precipitation methods, the morphology of Fe<sub>3</sub>O<sub>4</sub>-MWCNTs@PEI-Ag nanocomposite was somehow poor in comparison with high-temperature decomposition methods.<sup>43,65</sup> Corresponding EDX analysis was also performed (bottom) and revealed the presence of all of the anticipated elements.

Thermogravimetric analysis was used to further characterize the catalyst and to determine its thermal stability. TGA curve for the Fe<sub>3</sub>O<sub>4</sub>-MWCNTs@PEI-Ag composite is presented in Fig. 4.

The curve consists of two distinct weight loss stages, one from 250 to 440 °C which can be attributed to decomposition of PEI,<sup>66</sup> and the other from 440 to 700 °C due to decomposition of MWCNTs,<sup>67</sup> with a total weight loss of 57%. It could be deduced that Fe<sub>3</sub>O<sub>4</sub>-MWCNTs@PEI-Ag has enough stability to endure harsh conditions up to 250 °C.

In order to further characterize the Fe<sub>3</sub>O<sub>4</sub>-MWCNTs@PEI-Ag composite, XPS survey spectrum was recorded. In Fig. 5a, one

**Table 6** Chemoselective reduction reaction of nitriles to amines by Fe<sub>3</sub>O<sub>4</sub>-MWCNTs@PEI-Ag as catalyst

Entry <sup>a</sup>	Nitrile compound	Product	Yield <sup>b</sup> (%)
1			96%
2			94%
3			92%
4			88%
5			98%

<sup>a</sup> All of the reactions were carried out according to the general experimental procedure. <sup>b</sup> GC yield in comparison with authentic samples.





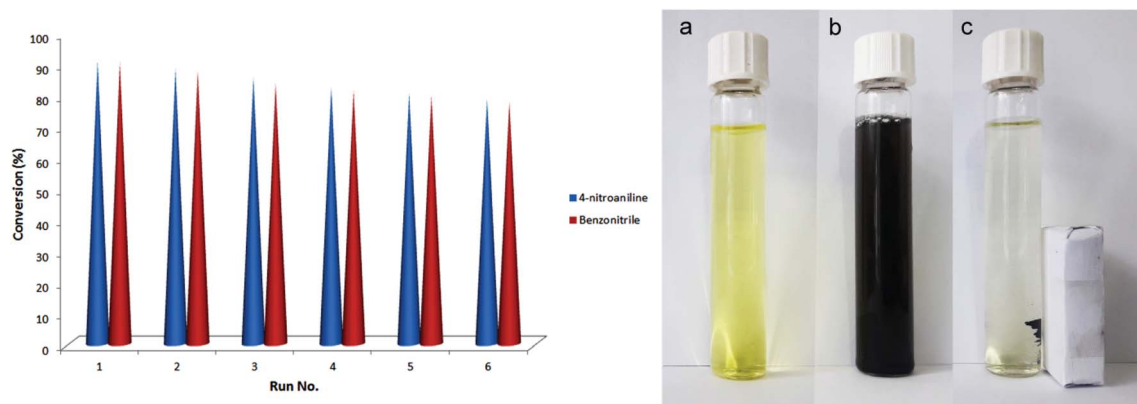


Fig. 9 Left: reusability of the  $\text{Fe}_3\text{O}_4\text{-MWCNTs@PEI-Ag}$  catalyst in reduction of 4-nitroaniline and benzonitrile. Right: photographs of the 4-nitroaniline solution before (a) and after (b) addition of the catalyst, and after magnetic separation of the catalyst (c). The magnet was enveloped with a piece of white paper for clarity.

can note the presence of signals attributed to the Fe, O, N, and C. In addition, inset of Fig. 5a shows a high-resolution core level signal of metallic Ag, in which  $\text{Ag } 3d_{3/2}$  and  $\text{Ag } 3d_{5/2}$  are clearly visible and the splitting of the 3d doublet is 6.0 eV. In the high resolution spectrum of Fe, on the other hand, the characteristic spin-orbit doublets of  $\text{Fe}^{2+}$  and  $\text{Fe}^{3+}$  and shakeup satellites are clearly visible, which are in agreement with the reported values (Fig. 5b).<sup>43,65</sup>

To further differentiate between Ag and  $\text{Fe}_3\text{O}_4$ , mapping analysis was performed and the results are presented in Fig. 6. Based on the obtained layered images, it is crystal clear that a uniform dispersion of Ag nanoparticles over the surface of the support was obtained.

The magnetic hysteresis curve for  $\text{Fe}_3\text{O}_4\text{-MWCNTs@PEI-Ag}$  composite was also obtained. As can be seen in Fig. 7, typical magnetization curve for  $\text{Fe}_3\text{O}_4\text{-MWCNTs@PEI-Ag}$  composite as a function of applied magnetic field at 300 K is shown. The  $\text{Fe}_3\text{O}_4\text{-MWCNTs@PEI-Ag}$  composite sample exhibited typical super paramagnetic behavior with a large saturation magnetization of  $63.6 \text{ emu g}^{-1}$ .

### Catalytic reduction of nitroaromatic and nitrile compounds

In order to study the effectiveness of  $\text{Fe}_3\text{O}_4\text{-MWCNTs@PEI-Ag}$  nanocatalyst in the reduction of aromatic nitro and nitrile compounds, 4-nitroaniline was used as a model substrate to determine the optimum reaction conditions including catalyst amount, pH, and amount of the reducing agent. Trend of reduction was monitored by UV-Vis spectroscopy. Table 1 represents the effect of the catalyst amount on the reduction of 4-nitroaniline in water at  $25^\circ\text{C}$ .

It is clear that presence of the catalyst is necessary for successful reduction of 4-nitroaniline. Increasing in the catalyst amount from 0.7 to 1.3 mg resulted in a non-linear increase in the yield. Therefore, 1.0 mg of the  $\text{Fe}_3\text{O}_4\text{-MWCNTs@PEI-Ag}$  nanocatalyst was selected as the optimum amount. Reduction of 4-nitroaniline at different pH was also investigated. It was found that maximum performance was affordable under neutral pH in the reduction of 4-nitroaniline (Table 2, entry 2). Fig. 8 shows the recorded UV-Vis spectra of the aqueous solution of 4-nitroaniline at pH 7.0 after 0, 2, 4, 8, 12 and 15 min. Clearly, intensity of the peak at 380 nm was decreased with

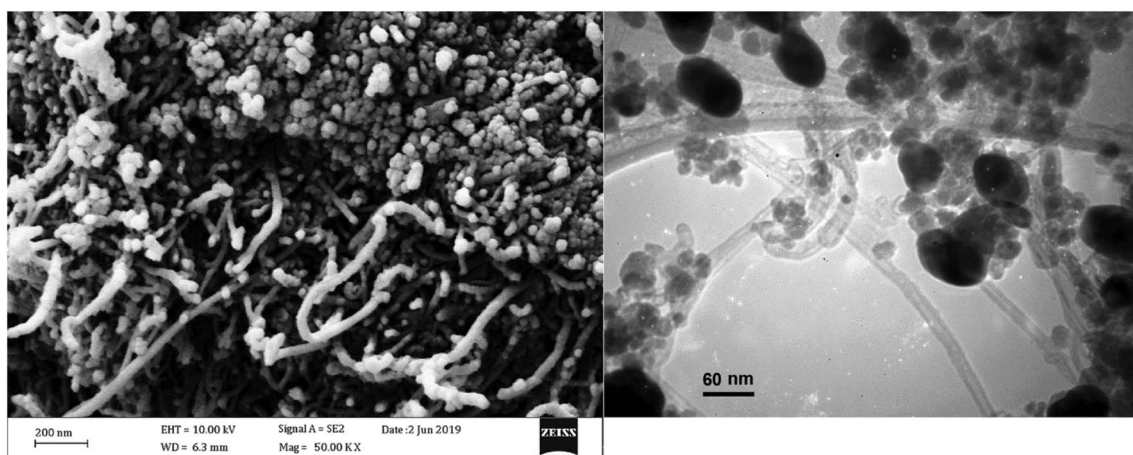


Fig. 10 SEM (left) and TEM (right) images of the recovered catalyst.



Table 7 A brief comparison of the results of the reduction of 4-nitroaniline (A) and benzonitrile (B) using different catalysts

Entry	Catalyst	Substrate	Catalyst amount per mmol of substrate (mg)	NaBH <sub>4</sub> (mmol)	Temp (°C)	Time (min)	Ref.
1	Fe <sub>3</sub> O <sub>4</sub> -MWCNTs@PEI-Ag	A	10	3	25	15	This work
		B	10	6	110	40	
2	Fe <sub>3</sub> O <sub>4</sub> @SiO <sub>2</sub> @KIT-6-Ag	A	100	111	25	17	74
		B	Not tested	—	—	—	
3	Au NPs (octahedral)	A	172.5	240	28	70	75
		B	Not tested	—	—	—	
4	Ag-RANEY® nickel	A	250	2	35	20	76
		B	Not tested	—	—	—	
5	Bi <sub>2</sub> S <sub>3</sub> microspheres	A	6000	1000	25	9	77
		B	Not tested	—	—	—	
6	Ag-PRGO	A	1000	132	25	4	78
		B	Not tested	—	—	—	
7	MNPs@PIL@AuNPs	A	5	10	25	70	79
		B	Not tested	—	—	—	

simultaneous outburst of a new peak at 240 nm which can be attributed to the formation of benzene-1,4-diamine.<sup>68</sup>

Effect of the amount of reducing agent was also studied, and the results are presented in (Table 3). Based on these results, 0.2 M of freshly prepared aqueous solution of sodium borohydride was selected as the optimum concentration.

In order to generalize the effectiveness of our catalyst under the optimum conditions, a variety of nitroaromatic compounds were reduced by NaBH<sub>4</sub> in presence of the Fe<sub>3</sub>O<sub>4</sub>-MWCNTs@PEI-Ag (Table 4). Since NaBH<sub>4</sub> concentration is much higher than the corresponding nitroaromatic compound, it can be assumed that the apparent rate constant follows a pseudo first-order kinetic because the concentration of NaBH<sub>4</sub> can be considered to be constant during the course of reduction. Therefore, the apparent rate constants for this method was determined as  $\ln C_t/C_0 = -kt$ , (where  $C_t$  is the residual and  $C_0$  is the initial concentration of the nitro compound).

These results clearly indicate that this methodology is pretty compatible with different functional groups. Even non-aromatic nitro compounds, such as nitrofurazone which is an antibiotic, undergo selective reduction to the corresponding aminofuran (Table 4, entry 4).

Nitrile hydrogenation, on the other hand, is another method to prepare amines. Strong hydride donors such as lithium aluminum hydride, or catalytic hydrogenation are the most commonly used approaches for this purpose.

Chemoselectivity however, is a major issue and in most studies, reduction of nitrile compounds to amides, secondary or tertiary amines has been reported.<sup>69–73</sup> Generally, less attention has been paid to the production of amines from nitrile compounds. In order to extend the application of Fe<sub>3</sub>O<sub>4</sub>-MWCNTs@PEI-Ag to the reduction of nitriles, we selected benzonitrile as a model substrate to determine the optimum reaction conditions with respect to the catalyst amount, reaction time, and temperature. Based on the data listed in Table 5, 10 mg of the catalyst per mmol of benzonitrile in water at 110 °C was selected as the optimum conditions. Under these circumstances, the reaction selectively afforded the expected product with excellent yield of 95% after 40 minutes.

To study the generality and scope, optimized reaction conditions were applied to various nitriles and satisfying results were obtained in each case with regard to chemoselectivity toward amines, and yield (Table 6).

Finally, we studied recyclability and reuse of the Fe<sub>3</sub>O<sub>4</sub>-MWCNTs@PEI-Ag catalyst. After completion of the reduction of 4-nitroaniline or benzonitrile, the catalyst was recovered and reused for six successive cycles without any significant decrease in its activity. Conversion percent values from run 1 to 6 were 90.7, 88.3, 85.5, 82.4, 80.5, and 78.7 for 4-nitroaniline, and 90.3, 87.5, 83.6, 81.4, 79.7, and 77.5 for benzonitrile (Fig. 9). To visualize the magnetic separation process, photographs of the 4-nitroaniline solution before and after addition of the catalyst, and after magnetic separation of the catalyst are also shown in Fig. 9.

It is noteworthy that the recovered catalyst from the 6<sup>th</sup> run of the 4-nitroaniline reduction reaction, to a large extent maintained its morphology. This can be understood from the following SEM and TEM images of the recovered catalyst Fig. 10.

To show the catalytic efficiency of Fe<sub>3</sub>O<sub>4</sub>-MWCNTs@PEI-Ag catalyst, we have compared our results for the reduction of nitro and nitrile aromatic compounds with other reported results for the same transformations (Table 7). shows that Fe<sub>3</sub>O<sub>4</sub>-MWCNTs@PEI-Ag combines some of the merits associated with other methods.

## Conclusions

In this study we have introduced Fe<sub>3</sub>O<sub>4</sub>-MWCNTs@PEI-Ag hybrid material as a heterogeneous catalyst for efficient reduction of a broad spectrum of nitro and nitrile compounds under mild conditions. It can be concluded that functionalization of the MWCNTs with PEI provided a suitable platform for coordination and *in situ* reduction of silver ions. Silver nanoparticles obtained from *in situ* reduction of Ag<sup>+</sup> ions, are responsible for the observed excellent chemoselectivity and yields. Although the mechanistic details of such transformations awaits further studies, preferential adsorption of the reactant on the catalyst through nitro group, may justify the obtained results, as was



investigated by Boronat *et al.*<sup>80</sup> In combination with magnetic properties of Fe<sub>3</sub>O<sub>4</sub>, Fe<sub>3</sub>O<sub>4</sub>-MWCNTs@PEI-Ag catalyst integrates various advantages such as chemoselectivity, thermal stability, ease of work-up, and above all, reusability, which are of interest from both environmental and economic point of view.

## Conflicts of interest

There are no conflicts to declare.

## Acknowledgements

Partial support of this study by research council of University of Guilan is gratefully acknowledged.

## References

- 1 P. Banerjee, M. Satapathy, A. Mukhopahayay and P. Das, *Bioresour. Bioprocess.*, 2014, **1**, 3.
- 2 K. Zheng, M. I. Setyawati, T.-P. Lim, D. T. Leong and J. Xie, *ACS Nano*, 2016, **10**, 7934–7942.
- 3 A. H. Alshehri, M. Jakubowska, A. Młodziński, M. Horaczek, D. Rudka, C. Free and J. D. Carey, *ACS Appl. Mater. Interfaces*, 2012, **4**, 7007–7010.
- 4 D. Chen, X. Mei, G. Ji, M. Lu, J. Xie, J. Lu and J. Y. Lee, *Angew. Chem., Int. Ed.*, 2012, **51**, 2409–2413.
- 5 S. Sarina, E. R. Wacławik and H. Zhu, *Green Chem.*, 2013, **15**, 1814–1833.
- 6 K. Fuku, R. Hayashi, S. Takakura, T. Kamegawa, K. Mori and H. Yamashita, *Angew. Chem., Int. Ed.*, 2013, **52**, 7446–7450.
- 7 L. Q. Xu, B. S. M. Yap, R. Wang, K.-G. Neoh, E.-T. Kang and G. D. Fu, *Ind. Eng. Chem. Res.*, 2014, **53**, 3116–3124.
- 8 C.-J. Zhong and M. M. Maye, *Adv. Mater.*, 2001, **13**, 1507–1511.
- 9 K. S. Shin, J.-Y. Choi, C. S. Park, H. J. Jang and K. Kim, *Catal. Lett.*, 2009, **133**, 1.
- 10 P. Zhang, C. Shao, Z. Zhang, M. Zhang, J. Mu, Z. Guo and Y. Liu, *Nanoscale*, 2011, **3**, 3357–3363.
- 11 T. Ji, L. Chen, L. Mu, R. Yuan, M. Knoblauch, F. S. Bao and J. Zhu, *Appl. Catal., B*, 2016, **182**, 306–315.
- 12 M. Horecha, E. Kaul, A. Horechyy and M. Stamm, *J. Mater. Chem. A*, 2014, **2**, 7431–7438.
- 13 B. Naik, V. S. Prasad and N. N. Ghosh, *Powder Technol.*, 2012, **232**, 1–6.
- 14 N. H. Khadry and M. A. Ghanem, *J. Mater. Chem.*, 2012, **22**, 12032–12038.
- 15 S. Tang, S. Vongehr and X. Meng, *J. Phys. Chem. C*, 2009, **114**, 977–982.
- 16 J. Liu, J. Wang, Z. Zhu, L. Li, X. Guo, S. F. Lincoln and R. K. Prud'homme, *AIChE J.*, 2014, **60**, 1977–1982.
- 17 H.-Y. Lee and M.-H. An, *Bull. Korean Chem. Soc.*, 2004, **25**, 1717–1719.
- 18 X. Yang, Y. Li, P. Zhang, R. Zhou, H. Peng, D. Liu and J. Gui, *ACS Appl. Mater. Interfaces*, 2018, **10**, 23154–23162.
- 19 Z. Zhang, C. Shao, P. Zou, P. Zhang, M. Zhang, J. Mu, Z. Guo, X. Li, C. Wang and Y. Liu, *Chem. Commun.*, 2011, **47**, 3906–3908.
- 20 S. A. Lawrence, *Amines: synthesis, properties and applications*, Cambridge University Press, 2004.
- 21 N. Ono, *The nitro group in organic synthesis*, John Wiley & Sons, 2003, vol. 9.
- 22 N. Gospodinova and L. Terlemezyan, *Prog. Polym. Sci.*, 1998, **23**, 1443–1484.
- 23 A. G. MacDiarmid, *Synth. Met.*, 1997, **84**, 27–34.
- 24 T. Tsukinoki and H. Tsuzuki, *Green Chem.*, 2001, **3**, 37–38.
- 25 B. Sreedhar, D. K. Devi and D. Yada, *Catal. Commun.*, 2011, **12**, 1009–1014.
- 26 P. Albers, K. Seibold, G. Prescher and H. Müller, *Appl. Catal., A*, 1999, **176**, 135–146.
- 27 G. Wienhoefer, M. Baseda-Krüger, C. Ziebart, F. A. Westerhaus, W. Baumann, R. Jackstell, K. Junge and M. Beller, *Chem. Commun.*, 2013, **49**, 9089–9091.
- 28 G. Wienhöfer, I. Sorribes, A. Boddien, F. Westerhaus, K. Junge, H. Junge, R. Llusar and M. Beller, *J. Am. Chem. Soc.*, 2011, **133**, 12875–12879.
- 29 P. S. Liu, *J. Org. Chem.*, 1987, **52**, 4717–4721.
- 30 B. Frank, M. Morassutto, R. Schomäcker, R. Schlögl and D. S. Su, *ChemCatChem*, 2010, **2**, 644–648.
- 31 B. Frank, J. Zhang, R. Blume, R. Schlögl and D. S. Su, *Angew. Chem., Int. Ed.*, 2009, **48**, 6913–6917.
- 32 J. Zhang, R. Wang, E. Liu, X. Gao, Z. Sun, F. Xiao, F. Girgsdies and D. S. Su, *Angew. Chem., Int. Ed.*, 2012, **51**, 7581–7585.
- 33 A. Yari and S. Derki, *Sens. Actuators, B*, 2016, **227**, 456–466.
- 34 Y. Chen and H. Gu, *Mater. Lett.*, 2012, **67**, 49–51.
- 35 B. Yoon, H.-B. Pan and C. M. Wai, *J. Phys. Chem. C*, 2009, **113**, 1520–1525.
- 36 M. Gopiraman, S. G. Babu, Z. Khatri, W. Kai, Y. A. Kim, M. Endo, R. Karvembu and I. S. Kim, *Carbon*, 2013, **62**, 135–148.
- 37 S. J. Tabatabaei Rezaei, H. Khorramabadi, A. Hesami, A. Ramazani, V. Amani and R. Ahmadi, *Ind. Eng. Chem. Res.*, 2017, **56**, 12256–12266.
- 38 M. R. Nabid, Y. Bide and S. J. T. Rezaei, *Appl. Catal., A*, 2011, **406**, 124–132.
- 39 V. Polshettiwar, R. Luque, A. Fihri, H. Zhu, M. Bouhrara and J.-M. Basset, *Chem. Rev.*, 2011, **111**, 3036–3075.
- 40 D. Wang and D. Astruc, *Chem. Rev.*, 2014, **114**, 6949–6985.
- 41 M. Zhang, J. Zheng, J. Wang, J. Xu, T. Hayat and N. S. Alharbi, *Sens. Actuators, B*, 2019, **282**, 85–95.
- 42 D. Zheng, M. Zhang, L. Ding, Y. Zhang, J. Zheng and J. Xu, *RSC Adv.*, 2016, **6**, 11973–11979.
- 43 M. Zhang, P. Xia, L. Wang, J. Zheng, Y. Wang, J. Xu and L. Wang, *RSC Adv.*, 2014, **4**, 44423–44426.
- 44 I. Ibrahim, J. Kalbacova, V. Engemaier, J. Pang, R. D. Rodriguez, D. Grimm, T. Gemming, D. R. T. Zahn, O. G. Schmidt and J. Eckert, *Chem. Mater.*, 2015, **27**, 5964–5973.
- 45 F. Shu, M. Wang, J. Pang and P. Yu, *Front. Chem. Sci. Eng.*, 2019, **13**, 393–399.
- 46 Y. Yin, J. Pang, J. Wang, X. Lu, Q. Hao, E. Saei Ghareh Naz, X. Zhou, L. Ma and O. G. Schmidt, *ACS Appl. Mater. Interfaces*, 2019, **11**, 15891–15897.
- 47 Y. Zhou, Y. Huang, J. Pang and K. Wang, *J. Power Sources*, 2019, **440**, 227149.



- 48 A. Soni, L. Zhao, H. Q. Ta, Q. Shi, J. Pang, P. S. Wrobel, T. Gemming, A. Bachmatiuk and M. H. Rummeli, *Nano-Struct. Nano-Objects*, 2018, **16**, 38–44.
- 49 Y. Deng, Z. Liu, A. Wang, D. Sun, Y. Chen, L. Yang, J. Pang, H. Li, H. Li and H. Liu, *Nano Energy*, 2019, **62**, 338–347.
- 50 F. Liu, L. Zeng, Y. Chen, R. Zhang, R. Yang, J. Pang, L. Ding, H. Liu and W. Zhou, *Nano Energy*, 2019, **61**, 18–26.
- 51 A. Hassankhani, S. M. Sadeghzadeh and R. Zhiani, *RSC Adv.*, 2018, **8**, 8761–8769.
- 52 F. Zhao, K. K. Khaing, D. Yin, B. Liu, T. Chen, C. Wu, K. Huang, L. Deng and L. Li, *RSC Adv.*, 2018, **8**, 42308–42321.
- 53 Y. Cao, X. Zhu, J. Jiang, C. Liu, J. Zhou, J. Ni, J. Zhang and J. Pang, *Sol. Energy Mater. Sol. Cells*, 2020, **206**, 110279.
- 54 Y. Cao, X. Zhu, H. Chen, X. Zhang, J. Zhou, Z. Hu and J. Pang, *Sol. Energy Mater. Sol. Cells*, 2019, **200**, 109945.
- 55 H. Ma, H. Zhang, M. Tong, J. Cao and W. Wu, *RSC Adv.*, 2019, **9**, 24751–24759.
- 56 M. Lu, Y. Chang, X.-H. Guan and G.-S. Wang, *RSC Adv.*, 2019, **9**, 33806–33813.
- 57 G.-T. Xia, C. Li, K. Wang and L.-W. Li, *Sci. Adv. Mater.*, 2019, **11**, 1079–1086.
- 58 R. Eisavi and A. Karimi, *RSC Adv.*, 2019, **9**, 29873–29887.
- 59 J. Safaei-Ghomi and Z. Omidshafiei, *RSC Adv.*, 2019, **9**, 37344–37354.
- 60 C. F. Wang, Y. C. Su, S. W. Kuo, C. F. Huang, Y. C. Sheen and F. C. Chang, *Angew. Chem., Int. Ed.*, 2006, **45**, 2248–2251.
- 61 M. R. Nabid, Y. Bide, E. Aghaghafari and S. J. T. Rezaei, *Catal. Lett.*, 2014, **144**, 355–363.
- 62 H. Wu, H. Shi, H. Zhang, X. Wang, Y. Yang, C. Yu, C. Hao, J. Du, H. Hu and S. Yang, *Biomaterials*, 2014, **35**, 5369–5380.
- 63 A. Gasnier, M. L. Pedano, F. Gutierrez, P. Labbé, G. A. Rivas and M. D. Rubianes, *Electrochim. Acta*, 2012, **71**, 73–81.
- 64 G. Guo, F. Qin, D. Yang, C. Wang, H. Xu and S. Yang, *Chem. Mater.*, 2008, **20**, 2291–2297.
- 65 M. Zhang, L. Chen, J. Zheng, W. Li, T. Hayat, N. S. Alharbi, W. Gan and J. Xu, *Dalton Trans.*, 2017, **46**, 9172–9179.
- 66 X. Xu, C. Song, J. M. Andresen, B. G. Miller and A. W. Scaroni, *Energy Fuels*, 2002, **16**, 1463–1469.
- 67 D. Dikio and N. Bixa, *Int. J. Appl. Chem.*, 2011, **7**, 35–42.
- 68 M. Kumar and S. Deka, *ACS Appl. Mater. Interfaces*, 2014, **6**, 16071–16081.
- 69 T. Mitsudome, Y. Mikami, H. Mori, S. Arita, T. Mizugaki, K. Jitsukawa and K. Kaneda, *Chem. Commun.*, 2009, 3258–3260.
- 70 J. Y. Zhang, X. P. Wang, H. Y. Liu, J. A. Tang and L. Jiang, *Colloids Surf., A*, 1998, **132**, 9–16.
- 71 G. S. Chauhan, R. Sharma and H. Lal, *J. Appl. Polym. Sci.*, 2004, **91**, 545–555.
- 72 S. Rivara, A. Lodola, M. Mor, A. Bedini, G. Spadoni, V. Lucini, M. Pannacci, F. Frascini, F. Scaglione and R. O. Sanchez, *J. Med. Chem.*, 2007, **50**, 6618–6626.
- 73 E. L. Downs and D. R. Tyler, *Coord. Chem. Rev.*, 2014, **280**, 28–37.
- 74 S. Ansari, A. Khorshidi and S. Shariati, *Catal. Lett.*, 2019, **149**, 410–418.
- 75 C.-Y. Chiu, P.-J. Chung, K.-U. Lao, C.-W. Liao and M. H. Huang, *J. Phys. Chem. C*, 2012, **116**, 23757–23763.
- 76 A. Khorshidi and B. Ghorbannezhad, *RSC Adv.*, 2017, **7**, 29938–29943.
- 77 F. Guo, Y. Ni, Y. Ma, N. Xiang and C. Liu, *New J. Chem.*, 2014, **38**, 5324–5330.
- 78 M.-Q. Yang, X. Pan, N. Zhang and Y.-J. Xu, *CrystEngComm*, 2013, **15**, 6819–6828.
- 79 F. M. Moghaddam, S. E. Ayati, H. R. Firouzi, S. H. Hosseini and A. Pourjavadi, *Appl. Organomet. Chem.*, 2017, **31**, e3825.
- 80 M. Boronat, P. Concepcion, A. Corma, S. Gonzalez, F. Illas and P. Serna, *J. Am. Chem. Soc.*, 2007, **129**, 16230–16237.

